Improving the connectivity of MgB_2 bulk superconductors by a novel liquid phase sintering process

OPEN ACCESS
IOP Publishing
Superconductor Science and Technology
Supercond. Sci. Technol. **35** (2022) 065005 (11pp)
https://doi.org/10.1088/1361-6668/ac5164

Improving the connectivity of MgB_2 bulk superconductors by a novel liquid phase sintering process

G A B Matthews*, T Mousavi, S Santra, C R M Grovenor, P S Grant and S Speller

Materials Department, University of Oxford, Parks Road, OX13PH Oxford, United Kingdom

E-mail: guillaume.matthews@materials.ox.ac.uk

Received 11 October 2021, revised 16 January 2022
Accepted for publication 2 February 2022
Published 26 April 2022

Abstract

This work investigates a new processing method developed to improve the connectivity of *ex-situ* MgB_2 bulks at low sintering temperatures. Mg additions (1–10 wt.%) were mixed to pre-synthesised MgB_2 to make composite powders that were sintered at 900 °C by the field assisted sintering technique. Addition of 10 wt.% Mg resulted in a substantial increase in density from 68% to 79% and a dramatic reduction in MgB_4 from 11 to ∼0 wt.%. Pressure and dilatometry data recorded *in-situ* during the sintering process revealed that Mg additions led to different sintering mechanisms depending on the Mg fraction. For large Mg fractions (6 and 10 wt.%) a Mg liquid phase was formed and led to significant density improvements, and all pre-existing MgB_4 was transformed into MgB_2. A small amount of residual Mg remained in the bulks after the sintering process. Connectivity was improved with Mg additions, increasing four fold in the 10 wt.% Mg-MgB_2 sample compared to unmodified MgB_2. J_c values at low field were also significantly improved by Mg additions, in particular the 6 and 10 wt.% Mg-MgB_2 specimens showed J_c(20 K, 0 T) values 4–5 times higher than for unmodified MgB_2.

Keywords: MgB_2, superconductor, liquid phase sintering, connectivity, critical current density, Mg additions, spark plasma sintering

(Some figures may appear in colour only in the online journal)

1. Introduction

MgB_2 is considered as a promising material in the field of applied superconductivity due to its relatively high critical temperature of 39 K (T_c) and the fact that MgB_2 can be manufactured in various forms (bulks, wires and tapes) by scalable and readily available powder metallurgy routes. Its high T_c value makes it more suitable for liquid helium-free applications than conventional low temperature superconductors (LTSs) such as NbTi and Nb_3Sn. In addition, MgB_2 does not contain any rare earth or toxic elements and is also much easier and cheaper to process than high temperature superconductors such as the cuprates [1]. This combination of properties makes MgB_2 an attractive candidate to replace 'traditional' LTS materials such as NbTi in applications including MRI machines and magnetic drug targeting devices [2, 3].

MgB_2 bulks and wires are routinely produced by various processing techniques commonly grouped in two categories: *in-situ* and *ex-situ* methods. In the case of the *in-situ* route, Mg and B precursor powders react together to form the MgB_2 phase at moderate temperatures (600 °C–900 °C). This method has the advantage of producing sintered specimens showing high inter-grain connectivity. On the other hand, the large density difference between the precursor powders (2.10 g cm^{-3} for the powder mixture compared to 2.63 g cm^{-3}

* Author to whom any correspondence should be addressed.

for MgB_2) leads to extremely porous specimens, which in turn reduces the total cross sectional area for supercurrents and also results in poor mechanical properties [4–6].

The *ex-situ* method, in which pre-synthesised MgB_2 powder is consolidated at high temperature (900°C–1300 °C), usually with the assistance of pressure, can produce samples with significantly higher density. The field assisted sintering technique (FAST), also known as Spark Plasma Sintering or Direct Current Sintering is a popular technique that has been used successfully to produce dense MgB_2 specimens by different research groups [7–11]. This technique consists in driving a high current (usually at a low voltage) through an assembly composed of a graphite die in which the powder is enclosed between two graphite punches. The large current going through the punches/die and the green compact (if conductive) leads to rapid heating and densification of the powder through Joule heating. Several groups have used sintering temperatures in excess of 1100 °C to obtain dense and well-connected MgB_2 samples [5, 8, 10–12]. However, using high sintering temperatures is costly and also promotes the formation of impurity phases such as MgB_4 that lowers the total superconducting fraction in MgB_2 bulks manufactured at high temperatures. This comes from the decomposition reaction $2MgB_{2(s)} \rightleftharpoons MgB_{4(s)} + Mg_{(g)}$ that occurs around 900 °C [13, 14]. Matthews *et al* [11] also showed that the fraction of MgB_4 in MgB_2 bulks sintered by FAST rapidly increased with higher sintering temperatures.

Therefore, the following challenge arises: how to improve the density and connectivity of *ex-situ* MgB_2 bulks without using high temperatures that promote the formation of impurities and increase the manufacturing cost. One possibility, explored by a few research groups is to use ultra-high pressure sintering techniques [15–17]. However, pressure of several GPa requires specialist industrial presses and is not desirable for large scale commercial production.

In this study, a novel approach that we developed to sinter pre-synthesised MgB_2 powder is reported.

Liquid phase sintering (LPS) has been used for decades to consolidate ceramic materials that are difficult to sinter by conventional methods [18–20]. In LPS, a liquid forms in the green body and enhances sintering by pulling the powder particles together through capillary force and by improving the atomic transport mechanisms responsible for densification.

The approach investigated here involves mixing a small fraction of elemental Mg with pre-synthesised MgB_2 in an attempt to enhance densification and improve connectivity in bulks sintered at low temperature. It is expected that Mg (which melts at 650 °C) can form a liquid phase during sintering and thus promote densification. Mg-MgB_2 composite powders were consolidated using the FAST with the aim of developing a LPS process to significantly enhance connectivity and reduce the impurity content in *ex-situ* MgB_2 bulks manufactured at low temperature.

Several research groups have investigated the effect of excess Mg in the case of MgB_2 bulks and wires produced by the *in-situ* process [21–25]. Zeng *et al* [21] and Ma *et al* [23] both produced MgB_2 bulk samples by using 10 wt.% of excess Mg and reported significant improvements in critical current density (approximately 2–3 fold increase at self field and 20 K) compared to their reference MgB_2 sample. Zeng *et al* [21] showed a reduction in MgO content with excess Mg and concluded that Mg facilitated the oxygen intake in the MgB_2 lattice, improving grain connectivity and thus enhancing J_c. Ma *et al* [23] measured significantly higher density and connectivity values in their bulk sample containing 10 wt.% excess Mg. They suggested that the J_c improvements resulted from higher density and grain connectivity. Zhang *et al* [24] and Guner *et al* [25] reported similar findings and concluded that excess Mg led to higher density and lower impurities content in the bulk improving inter-grain connectivity and J_c values at low field.

Whereas the use of excess Mg is well documented in the case of the *in-situ* method, a process combining the *ex-situ* technique and Mg additions to promote LPS has not been investigated. In this work, a new method to consolidate *ex-situ* MgB_2 is presented and particular focus is given to the role of Mg in the sintering process and its effect on the microstructure and superconducting properties of *ex-situ* Mg-MgB_2 bulks.

2. Experimental details

Pre-synthesised MgB_2 (purity: 99%, Alfa Aesar) and elemental Mg (purity: 99.8%, Alfa Aesar) powders were mixed together manually for 5 min in a glovebox under Ar. Five compositions were investigated: the commercial MgB_2 powder and blends containing 1, 3, 6 and 10 wt.% Mg. The commercial and composite (Mg-MgB_2) powders were placed into a 20 mm diameter graphite die protected with graphite paper and two graphite punches were used to complete the assembly. Cold compaction of the powder was performed in the graphite die by using a uni-axial press that was operated to reach a pressure of 30 MPa for 1 min. The die assembly was then transferred into a Dr Fritsch DSP 507 FAST apparatus. Prior to sintering, the chamber was evacuated and then filled with Ar three times, to eliminate any residual oxygen in the chamber. The consolidation chamber was then continuously evacuated during the sintering process and a baseline pressure of approximately 0.4–0.6 mbar was obtained. The green bodies were heated from room temperature to 900 °C at a rate of 120 °C min^{-1} before being maintained at this temperature for 5 min. During this first heating step, the pressure was gradually increased to 50 MPa and then maintained during the 5 min dwell at 900 °C, before being progressively released during the final cooling step. The FAST apparatus was operated with a constant voltage and pulsed current ranging between 1.5–4 V and 0.4–1.2 kA.

The consolidated disks were typically 20 mm in diameter and 3–5 mm in thickness, and were characterised by several techniques, including x-ray diffraction (XRD), scanning electron microscopy (SEM), scanning transmission electron microscopy (STEM) and magnetometry. XRD patterns were acquired using a PANalytical Empyrean diffractometer with

$Cu_{k\alpha}$ radiation ($\lambda = 0.154$ nm) at 40 kV and 40 mA. The lattice parameter, crystallite size, strain and weight fraction of the different phases detected in the bulk specimens were estimated from the XRD data by using Rietveld refinement (PANalytical HighScore Plus software). The weight fraction was estimated by using the Hill and Howard method [26]. Instrumental broadening of peaks was corrected using a Si standard analysed under the same scan conditions. The SEM analysis was undertaken in a Zeiss Merlin field emission gun SEM system operating at 10 kV, equipped with an Oxford Instrument 150 mm^2 Xmax EDX detector. The STEM analysis was performed in a JEOL 3000F at an accelerating voltage of 300 kV, equipped with a high angle annular dark field (HAADF) detector and an Oxford Instrument EDX detector. STEM specimens were prepared by cutting 3 mm disks from thin slices obtained from the sintered pellets. The disks were then mechanically polished to approximately 100 μm before being dimpled and finally thinned to perforation with a Fischione 1010 Ion Mill. The bulk density of the consolidated pellets was measured in isopropanol using the Archimedes' method. Magnetisation measurements were acquired with a Quantum Design physical property measurement system vibrating sample magnetometer on cuboid samples with dimensions of approximately 2 $\times$ 2 $\times$ 3 mm. The critical current density (J_c(B)) was estimated from the full magnetic hysteresis loops using Bean's model [27].

To estimate the effective cross-sectional area for macroscopic current transport in the bulk samples, four-point transport measurements and analysis of connectivity have been performed to obtain the normal state electrical resistivity as a function of temperature. Following the analysis of Collings *et al* [28], values of connectivity were extracted from the data using the procedure described in a previous article by Matthews *et al* [11]. The Materials constant K used in the connectivity analysis was estimated by fitting reference single crystal data from Eltsev *et al* [29].

3. Results and discussion

3.1. XRD and density measurements

Figure 1 shows the XRD patterns for 3 and 10 wt.% Mg-MgB_2 and unmodified MgB_2 sintered by FAST. Mg additions had a dramatic effect on the composition of the consolidated samples, in particular on the fractions of residual Mg and MgB_4.

To quantify the phase compositions, XRD patterns of all five specimens have been analysed by Rietveld refinement and the results are summarised in table 1. The fraction of MgO was identical in all four Mg-MgB_2 specimens and unmodified MgB_2. In contrast, the amount of MgB_4 decreased drastically in samples containing Mg additions, from >10% by weight to a level that was undetectable in the 6 and 10 wt.% specimens. In fact, these two samples contained 0.4 and 4 wt.% of residual Mg respectively. The evolution of the composition with Mg additions is also shown graphically in figure 2. This can be explained by applying Le Chatelier's principle to the decomposition reaction $2MgB_{2(s)} \rightleftharpoons MgB_{4(s)} + Mg_{(g)}$. Le Chatelier's principle states that if a dynamic equilibrium is disturbed by a change in the reaction conditions, the position of the equilibrium moves to counteract this change. In the absence of Mg additions, the forward reaction is favoured and MgB_2 decomposes into $MgB_{4(s)}$ and $Mg_{(g)}$ until the dynamic equilibrium for these particular conditions is reached. Indeed, table 1 shows that the sample consolidated from unmodified MgB_2 contained 11 wt.% MgB_4. However, in the samples containing Mg additions, presumably some Mg evaporated and created a positive pressure of $Mg_{(g)}$ thus moving the dynamic equilibrium of the decomposition reaction to the left.

XRD characterisation of the as-received MgB_2 powder showed that it contained 7 wt.% MgB_4 prior to sintering. This means that in the Mg-MgB_2 samples containing 3, 6 and 10 wt.% Mg, Mg additions not only suppressed MgB_2 decomposition but reacted with pre-existing MgB_4 to form 'fresh' MgB_2 during sintering. In other words, Mg additions converted pre-existing MgB_4 impurities into MgB_2 *in-situ*.

The pressure data recorded while sintering Mg-MgB_2 samples provided valuable insight on the reactions that occurred during sintering. Figure 3 shows the pressure in the sintering chamber as a function of temperature during the first heating step. Unmodified MgB_2 powder showed a broad peak in pressure at 600 °C–800 °C which corresponds to the MgB_2 decomposition reaction. This is in good agreement with the Mg-B phase diagram calculated by Liu *et al* [13] at 1 Torr showing that Mg starts evaporating from MgB_2 above 600 °C. In contrast, this broad peak was not observed in the samples containing Mg additions. Instead, a narrower peak was detected at 500 °C–600 °C which corresponds to Mg evaporation from the Mg additions. This is consistent with the works of Coleman and Egerton [30] and Moser *et al* [31] who showed that the Mg vapour pressure over solid Mg rose steeply above approximately 500 °C. These results suggest that metallic Mg evaporated at lower temperatures and formed a positive $Mg_{(g)}$ pressure within the green body that suppressed the evaporation of Mg from MgB_2, thus eliminating its decomposition. This is in good agreement with the XRD results and confirms the theoretical explanation based on Le Chatelier's principle, which is also consistent with the Mg-B phase diagram [13].

Table 1 shows that the Mg-MgB_2 sample containing 1 wt.% Mg had almost the same density as unmodified MgB_2. This suggests that most of the metallic Mg probably evaporated during sintering and did not significantly enhance densification. However, the Mg-MgB_2 samples with larger Mg additions showed a significant increase in density, reaching 79% in the 10 wt.% Mg-MgB_2 sample compared to 68% in unmodified MgB_2. This indicates that for higher Mg concentrations, not all metallic Mg evaporated and some Mg formed a liquid phase that enhanced diffusion rates leading to faster densification. In order to confirm this theory, the piston travel data has been analysed for the Mg-MgB_2 samples and unmodified MgB_2. Figure 4 shows the relative piston travel as a function of temperature during the first heating step of the sintering program. In unmodified MgB_2, the curve has two distinct parts: a linear decrease between room temperature and 800 °C followed by a sudden drop above 800 °C. The first part corresponds to the compaction of the powder due to the pressure

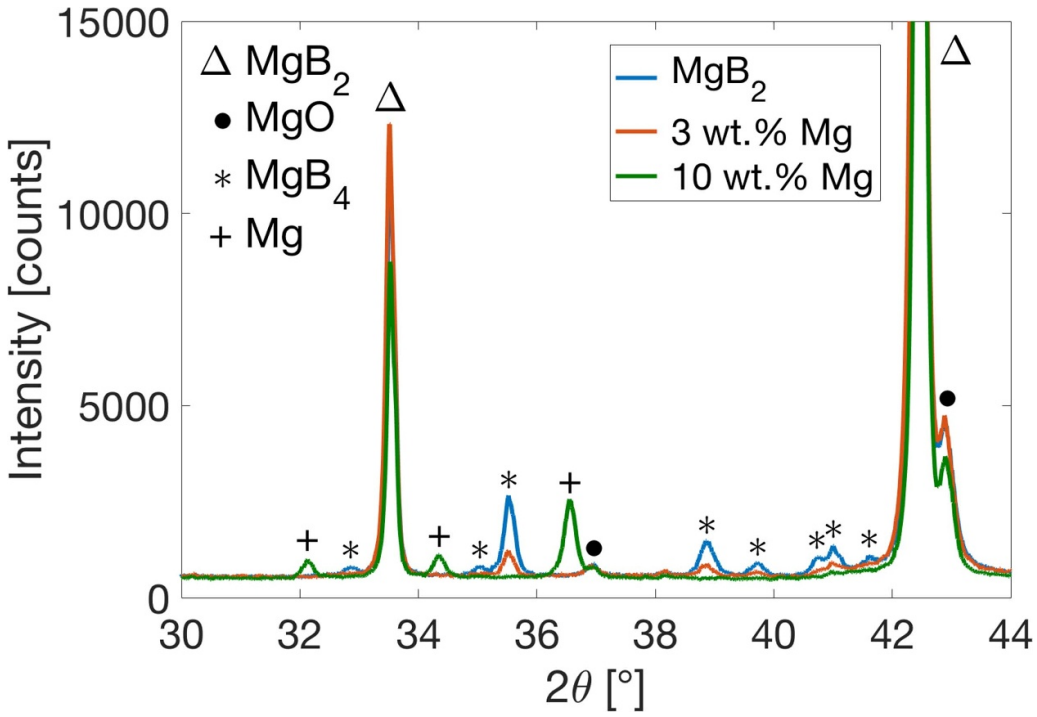

Figure 1. XRD patterns for Mg-MgB_2 samples and unmodified MgB_2.

Table 1. XRD characterisation and density measurements of Mg-MgB_2 composite bulk samples manufactured by FAST. *No MgB_4 or Mg peaks were detected.

Sample	MgO (wt.%)	MgB_4 (wt.%)	Mg (wt.%)	Relative density (%)	MgB_2 crystallite size (nm)	MgB_2 strain (%)	MgO crystallite size (nm)	MgB_2 *a*-axis (Å)	MgB_2 *c*-axis (Å)
MgB_2 powder	5	7	—	—	100	0.11	—	3.086	3.524
MgB_2	7	11	—	68	120	0.12	30	3.085	3.525
1 wt.%	8	9	0*	69	120	0.12	30	3.085	3.525
3 wt.%	8	4	0*	72	120	0.12	34	3.085	3.525
6 wt.%	8	0*	0.4	76	130	0.10	39	3.085	3.523
10 wt.%	8	0*	4	79	130	0.10	44	3.085	3.523
Precision	±0.4	±1.3	—	±1	±12	±0.005	±4	$\pm 2 \times 10^{-4}$	$\pm 3 \times 10^{-4}$

which increased linearly from room temperature to reach 50 MPa at 900 °C. The second part corresponds to sintering of the powder with the onset of sintering at 800 °C.

The curve of the 1 wt.% sample was almost identical to unmodified MgB_2 with the onset of sintering also located at 800 °C. This is in good agreement with the density measurements and confirms that all the Mg evaporated at lower temperatures and did not form a liquid phase. In contrast, the composite specimens with larger Mg additions showed very different sintering curves. The 3 wt.% sample had a very similar curve to unmodified MgB_2 up to 600 °C–650 °C, but then diverged significantly and showed a rapid decrease above 600 °C–650 °C. The onset of sintering was thus pushed to lower temperatures, around 600 °C–650 °C, which coincides with the melting temperature of Mg at 650 °C. This suggests that Mg formed a liquid phase and enhanced densification, as shown in table 1. The 6 and 10 wt.% specimens showed a travel curve similar to the 3 wt.% sample, only slightly shifted downward indicating better compaction due to the higher Mg content, and with the onset of sintering also located at lower temperatures compared to unmodified MgB_2. This confirms that the sintering behaviour is modified with the addition of sufficient ($\geq$3 wt.%) metallic Mg.

Table 1 shows that all four Mg-MgB_2 samples and unmodified MgB_2 had very similar MgB_2 crystallite size which suggests that Mg additions did not affect the MgB_2 coarsening rate. All five samples also had similar inhomogeneous strain values and *a* and *c*-axis lattice parameters. However, the MgO crystallite size increased with higher Mg concentrations, reaching 44 nm in the 10 wt.% sample compared to 31 nm for unmodified MgB_2. Since all the composite specimens and unmodified MgB_2 had the same MgO content, this suggests that the liquid Mg phase slightly increased MgO coarsening rate during the sintering process.

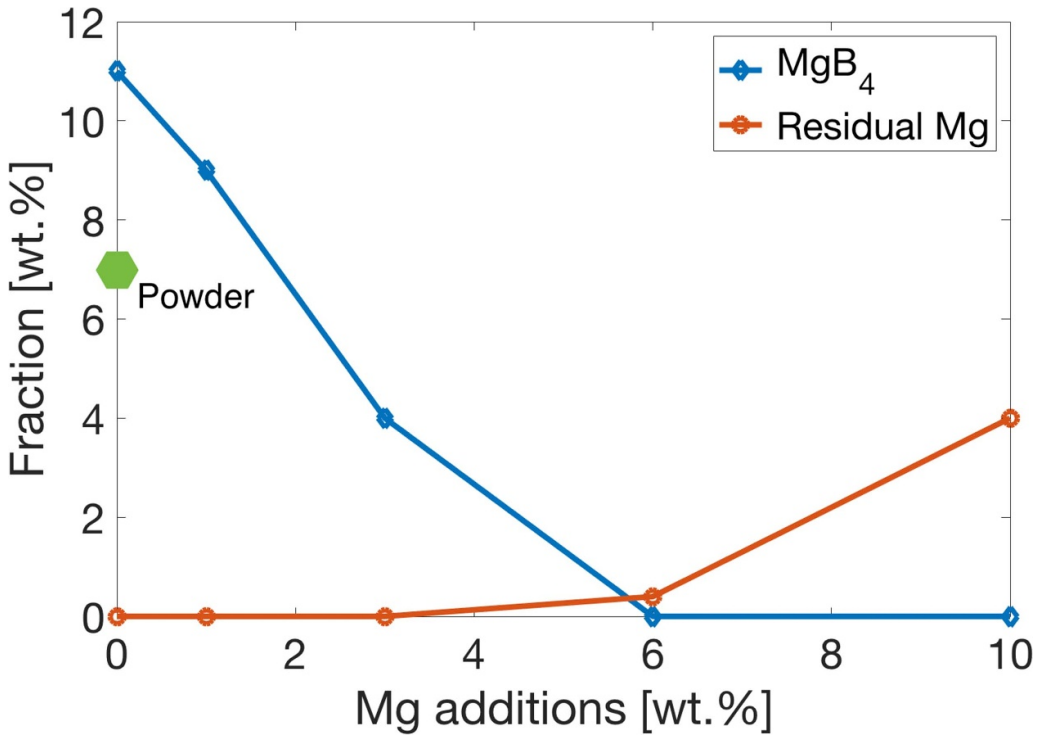

Figure 2. Fraction of MgB_4 and residual Mg estimated by XRD analysis for Mg-MgB_2 samples and unmodified MgB_2. The fraction of pre-existing MgB_4 in the commercial MgB_2 powder is shown by the green hexagon.

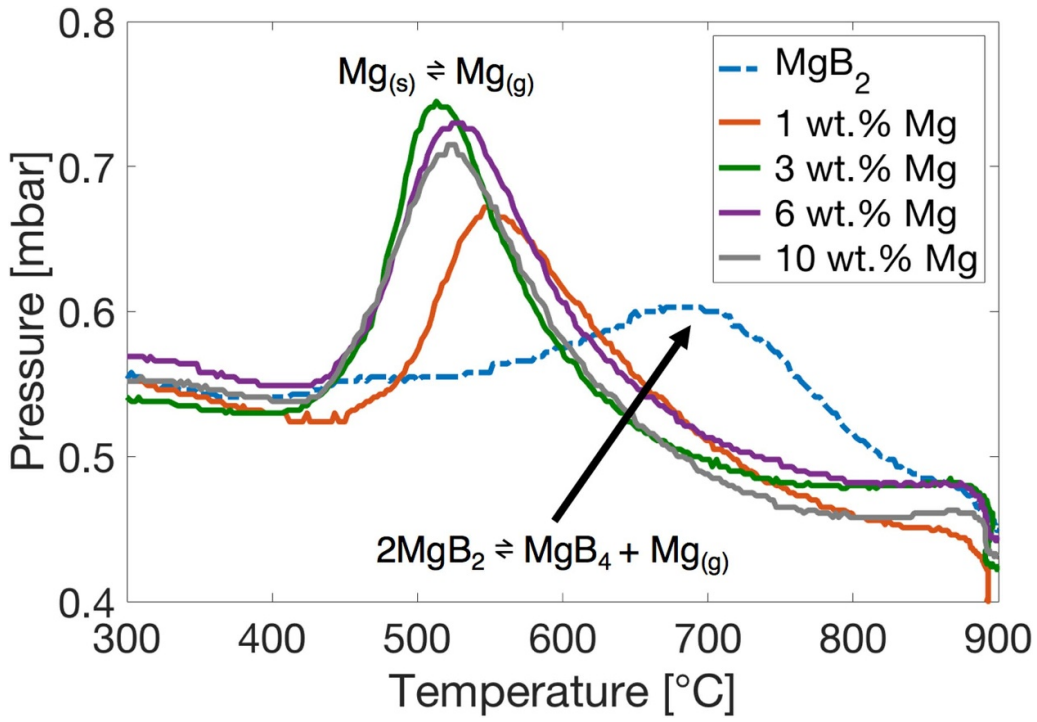

Figure 3. Pressure in the FAST chamber during the heating step of the sintering process. Data is shown for Mg-MgB_2 samples and unmodified MgB_2.

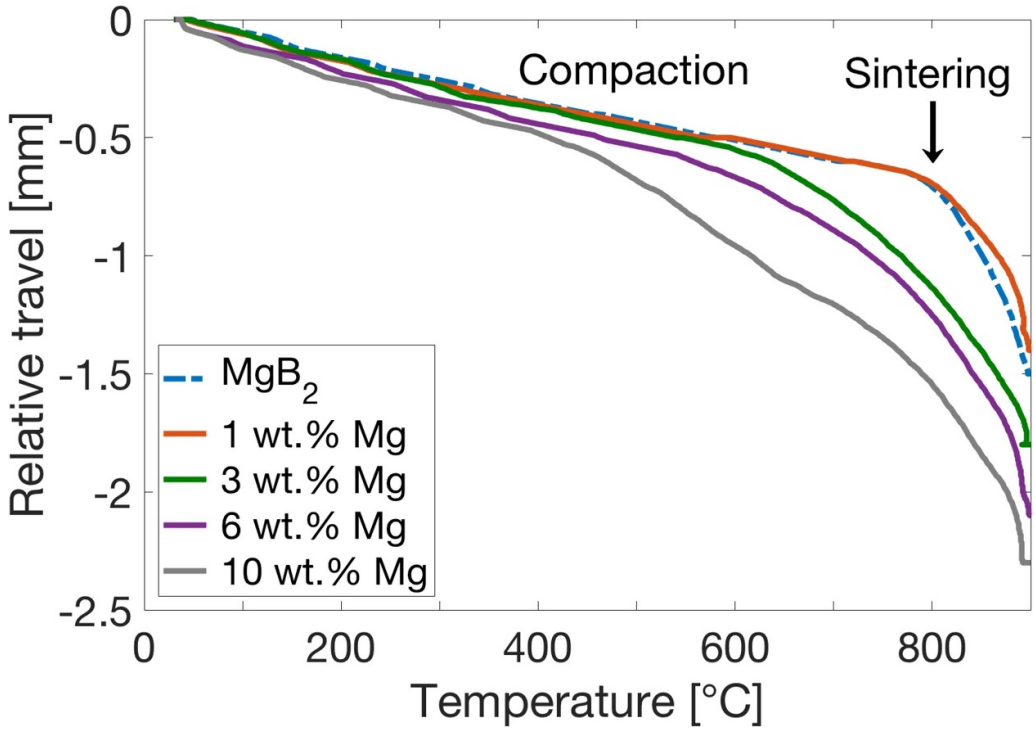

Figure 4. Relative travel of the piston during the heating step of the sintering process. Data is shown for Mg-MgB_2 samples and unmodified MgB_2. The data was smoothed for better legibility.

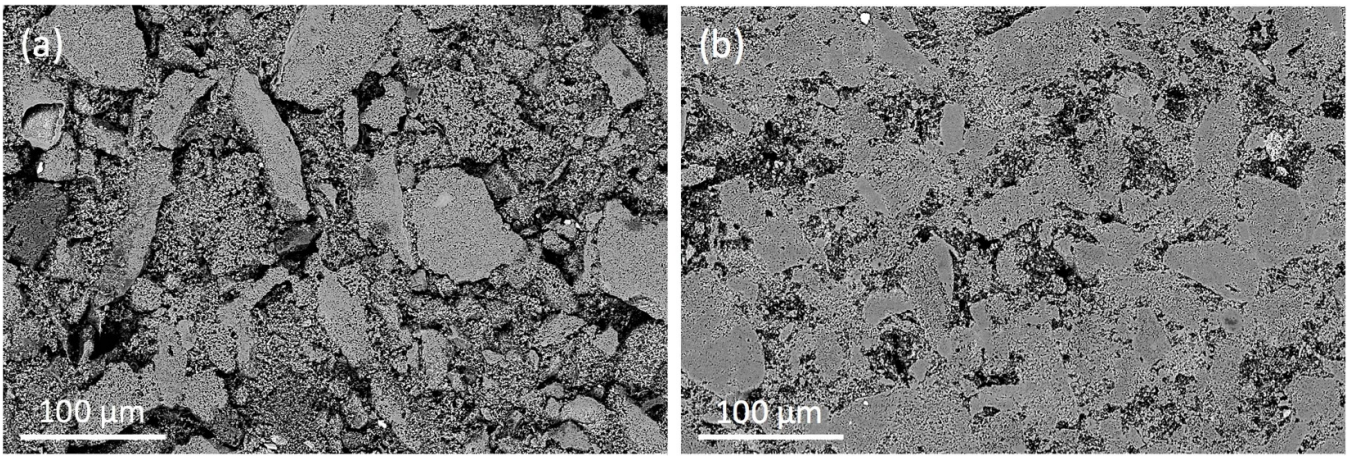

Figure 5. Typical backscattered SEM images for (a) unmodified MgB_2 and (b) 10 wt.% Mg-MgB_2 sintered 5 min at 900 °C by FAST. The samples were ground and polished with a diamond suspension.

3.2. SEM and STEM analysis

Figure 5 shows typical low magnification backscattered SEM images for unmodified MgB_2 and the 10 wt.% Mg-MgB_2 sample. Unmodified MgB_2 sintered at 900 °C did not show any sign of sintering and had a very porous microstructure. In contrast, the Mg-MgB_2 sample showed a much more connected microstructure and less porosity, indicating that densification was significantly enhanced compared to unmodified MgB_2. This is in good agreement with the large increase in density observed for the Mg-MgB_2 sample. No MgB_4 could be seen by SEM, which is consistent with the XRD results (table 1). However, the XRD analysis indicated the presence of residual Mg (∼4 wt.%), but Mg could not be detected by SEM and EDX mapping. This could come from a lack of backscattered electron contrast between the Mg and MgB_2 phase or the fact that Mg regions were too small to be resolved by EDX.

Ceramics based on the Si_3N_4 or SiC structures are sintered using LPS by adding metal oxides and/or nitrides which react with the surface silica present in the starting powder to form a liquid phase that acts as a transport medium and thus promotes densification. Liquid phase sintered Si_3N_4 and SiC usually contain thin films (few nm) of residual glassy material at the grain boundaries and larger pockets (few tens of nm) at triple grain junctions [32].

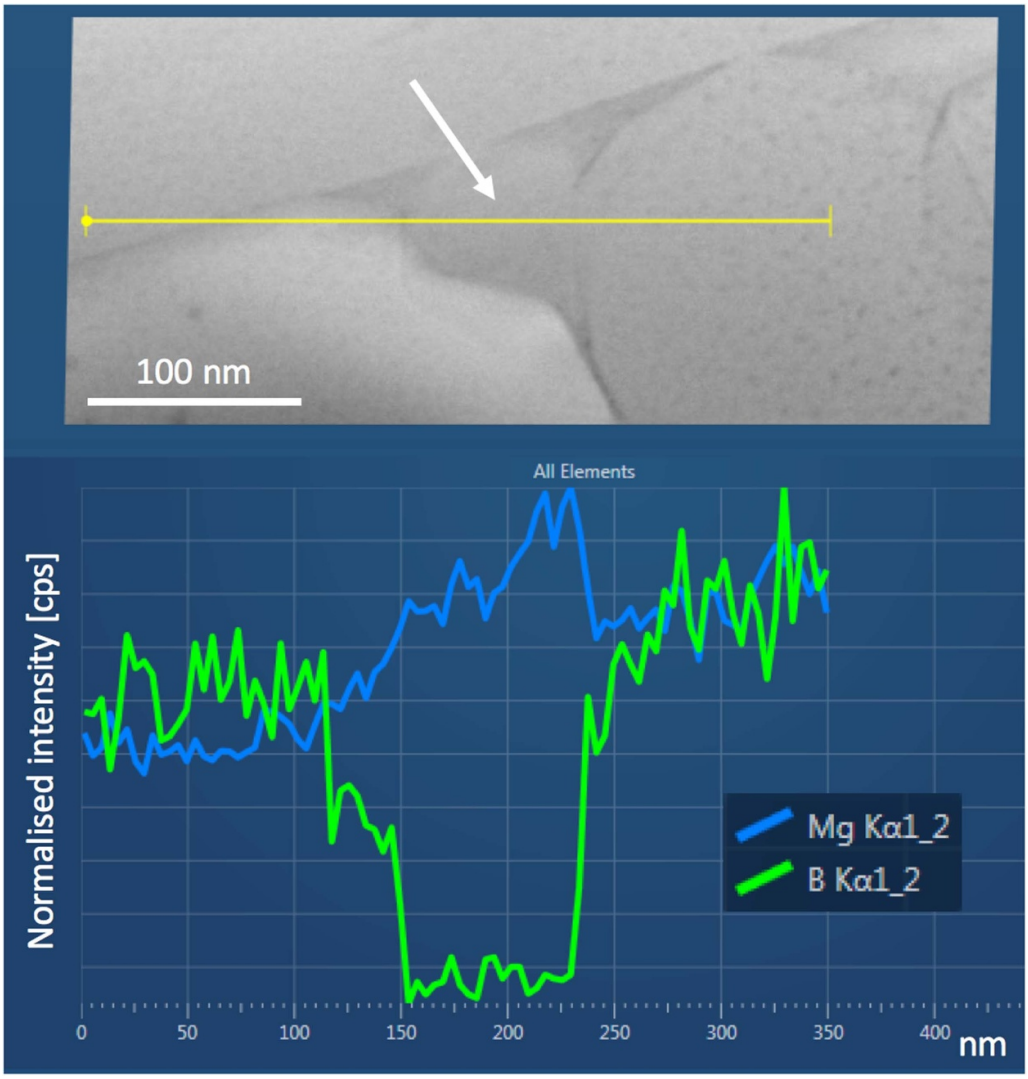

Figure 6. Typical STEM HAADF image of 10 wt.% Mg-MgB_2 showing a triple grain junction (arrow). An EDX linescan was performed across the triple grain junction.

It was shown above that Mg melted during the sintering process and also promoted densification. Therefore, similar to the glassy phase found in LPS Si_3N_4 and SiC, Mg in Mg-MgB_2 samples could also form thin layers at the grain boundaries and/or small pockets of residual Mg at triple grain junctions. Such small features cannot be resolved by SEM, but TEM/STEM analysis could confirm the presence of residual Mg.

The 10 wt.% Mg-MgB_2 specimen was further analysed by STEM, and figure 6 shows a typical HAADF image depicting a triple grain junction (indicated by the arrow) and an EDX linescan running through the small pocket located at the junction. The pocket is richer in Mg and depleted in B, which supports the theory that Mg forms a liquid phase during sintering with some residual Mg forming pockets at triple grain junctions. This is consistent to what is observed in liquid phase sintered Si_3N_4 and SiC [32].

3.3. Microstructural evolution during the LPS process

A model for this new LPS process was developed by combining all the characterisation results presented above in order to provide an accurate description of the microstructural evolution during the sintering of MgB_2 bulks containing different fractions of Mg additions (1 up to 10 wt.%) The effects of Mg additions can be summarised as follow:

- 1 wt.%: Metallic Mg evaporated during sintering and generated a positive $Mg_{(g)}$ pressure which modified the dynamic equilibrium of the MgB_2 decomposition reaction causing less MgB_4 to be formed. No liquid phase was formed and thus no increase in density was observed compared to unmodified MgB_2.
- 3 wt.%: Some Mg evaporated and MgB_2 decomposition was suppressed. A liquid phase was formed which enhanced

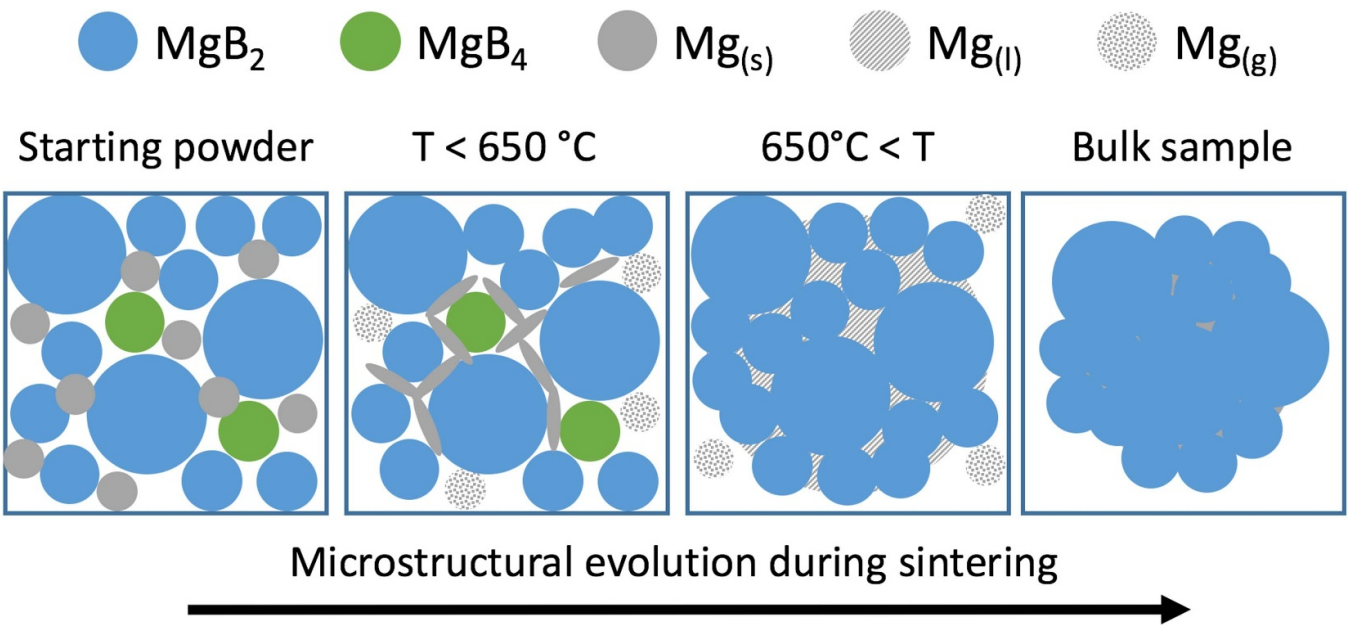

Figure 7. Schematic showing the evolution of the microstructure during LPS of Mg-MgB_2 samples containing >6 wt.% Mg.

densification and also reacted with pre-existing MgB_4 to form 'fresh' MgB_2. No residual Mg was detected and the density increased compared to unmodified MgB_2. In addition, a reduction in the MgB_4 fraction compared to the as-received MgB_2 powder was observed.

- 6 wt.%: More liquid phase was formed and led to further density improvements and reduction in MgB_4. No MgB_4 was detected and a very small amount (0.4 wt.%) of residual Mg remained in the bulk after the sintering process.
- 10 wt.%: The large volume fraction of Mg led to better compaction at low temperature. A liquid phase was then formed at higher temperature and led to further improvements in density. No MgB_4 was detected and a larger fraction of residual Mg (4 wt.%) was present in the sample. The different steps of the LPS process are presented schematically in figure 7.

3.4. Magnetic measurements

Zero field cooled measurements in figure 8(a) show that the superconducting transition becomes narrower with increasing Mg additions. ΔT_c decreased from 1.7 K in unmodified MgB_2 to 0.6 K in the sample containing 10 wt.% Mg, as shown in table 2. Matthews *et al* [11] reported a similar reduction in ΔT_c in unmodified MgB_2 samples sintered at higher temperature. The authors attributed this to heterogeneities (composition and/or disorder) initially present in the as-received powder being annealed out at high temperature. Here, all four samples were sintered at 900 °C suggesting that the reduction in ΔT_c is an effect of the Mg additions. Higher sintering temperatures and larger Mg fractions both lead to an increase in the diffusion rate, as suggested by the higher density of the 10 wt.% Mg-MgB_2 sample. In addition, it is also likely that as-received MgB_2 powder contained defects and/or local chemical heterogeneities which resulted in the relatively large ΔT_c value in the sample made from unmodified MgB_2. A possible explanation for the effect of Mg additions on ΔT_c could be that even though the sintering temperature is low (900 °C) the higher diffusion rate provided by liquid Mg during sintering acts to smooth chemical heterogeneities and thus makes the sample more homogeneous, reducing ΔT_c.

Figure 8(b) shows that the $J_c - B$ curves for the 1 and 3 wt.% Mg samples at 4.2 K seems to be simply translated vertically compared to unmodified MgB_2, maintaining a very similar shape. The $J_c - B$ curve of the 6 wt.% Mg sample was very similar to the 3 wt.% specimen at high field (>5 T), but J_c values at low field were further improved. On the other hand, the 10 wt.% sample showed a relatively different shape; low field J_c values were similar to the 6 wt.% specimen, but high field J_c was substantially reduced compared to unmodified MgB_2 and all three Mg-MgB_2 samples containing lower Mg additions. The 10 wt.% sample also had an irreversibility field B_{irr} approximatively 1.5 T lower than the other four specimens, as shown in table 2. This suggests that the MgB_2 lattice of the 10 wt.% sample was 'cleaner' (following the definition of Anderson [33]). As discussed earlier, the 10 wt.% sample was the only specimen to contain a significant fraction of residual Mg (~4 wt.%) after the sintering process, and also showed the largest increase in density, attributed to the effect of Mg acting as a liquid phase during consolidation. It is known that the liquid phase in Si_3N_4 and SiC acts as an impurity sink due to the much larger solubility of impurities in the liquid phase than in the solid phase [32]. It is possible that the Mg liquid phase during sintering also acts as an impurity sink and thus makes the MgB_2 lattice 'cleaner', explaining the significant reduction in B_{irr} observed in the 10 wt.% Mg-MgB_2 bulk. Another possibility is that flux pinning in the 10 wt.% Mg sample is not as good as in bulks containing less Mg additions.

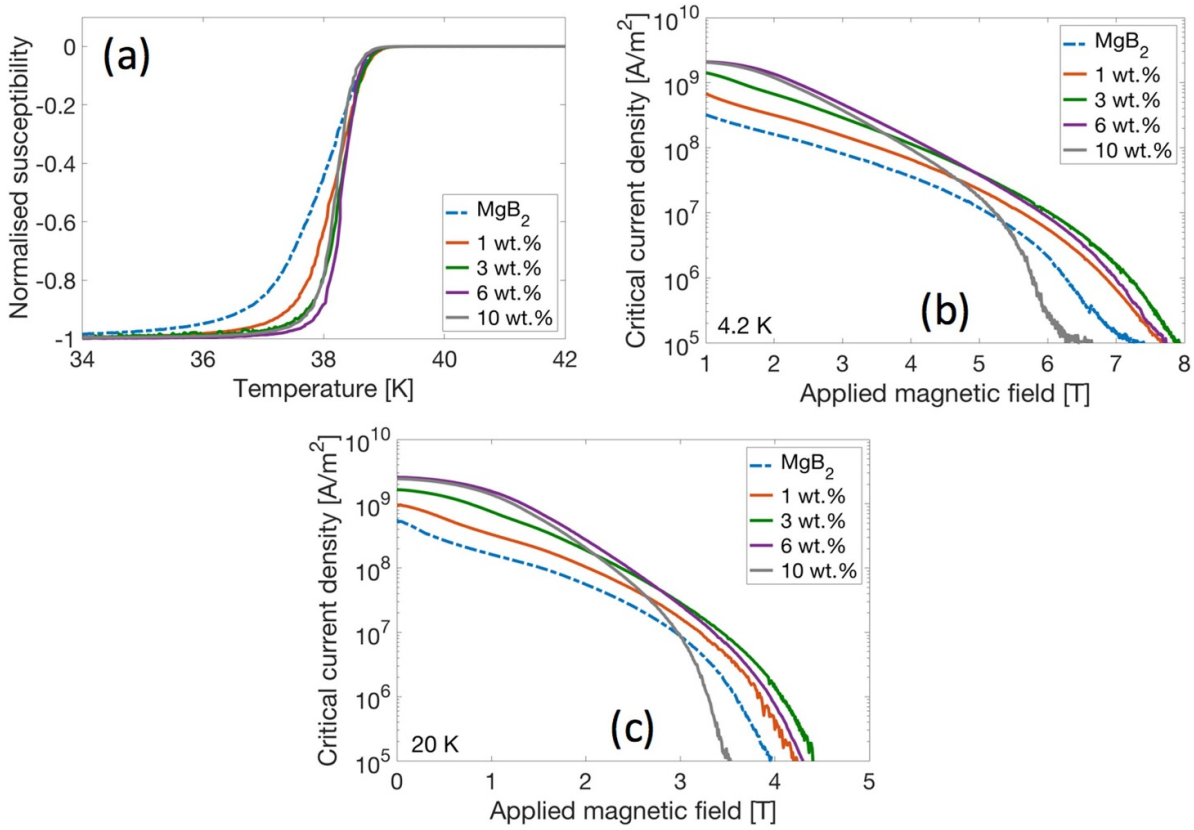

Figure 8. Superconducting properties of unmodified MgB_2 and Mg-MgB_2 samples containing 1, 3, 6 and 10 wt.% Mg.

Table 2. Superconducting properties of unmodified MgB_2 and Mg-MgB_2 samples containing 1, 3, 6 and 10 wt.% Mg. J_c values were estimated using the macro-scale model.

Sample	$T_{c,onset}$ (K)	ΔT_c (K)	B_{irr}(4.2 K) [T]	B_{irr}(20 K) [T]	J_c(5 T, 4.2 K) (A m^{-2})	J_c(0 T,20 K) (A m^{-2})
MgB_2	38.6	1.7	6.8	3.8	1.2×10^7	0.55×10^9
1 wt.%	38.6	1.1	6.8	3.9	2.3×10^7	1×10^9
3 wt.%	38.6	0.7	7	3.9	3.9×10^7	1.7×10^9
6 wt.%	38.6	0.6	7	3.8	3.8×10^7	2.6×10^9
10 wt.%	38.5	0.6	5.4	3.1	1.8×10^7	2.4×10^9

However, table 1 shows that the 6 and 10 wt.% Mg samples, although having different B_{irr}, have very similar MgB_2 and MgO crystallite size and the same MgO fraction, suggesting similar pinning environments.

At 20 K, the evolution of the $J_c - B$ curves with increasing Mg additions is very similar to that observed at 4.2 K. Self field J_c(20 K) increased more than four fold by adding 6 and 10 wt.% Mg compared to unmodified MgB_2. This is consistent with the SEM analysis (figure 5) showing that the microstructure of the 10 wt.% Mg sample sintered to a much greater extent than unmodified MgB_2.

3.5. Connectivity measurements

Figure 9 shows that connectivity increased significantly with Mg additions compared to unmodified MgB_2. In particular, the connectivity increased from only 6% in unmodified MgB_2 up to 25% in the sample containing 10 wt.% Mg. This increase in connectivity almost exactly matches the increase in self field J_c(20 K) discussed above. A strong correlation between connectivity and self field J_c values was also observed by Matthews *et al* [11] in unmodified MgB_2 sintered at temperatures ranging from 900 °C to 1200 °C. This confirms that connectivity has a significant effect on J_c values at low field, and also suggests that connectivity can be improved by using Mg additions instead of higher sintering temperatures. The 10 wt.% Mg specimen showed the best connectivity, suggesting that if there is a layer of residual Mg at grain boundaries it must be sufficiently thin not to adversely affect connectivity, which is consistent with the STEM analysis. The residual resistivity also decreased with increasing Mg fractions, indicating that Mg additions made the MgB_2 phase cleaner.

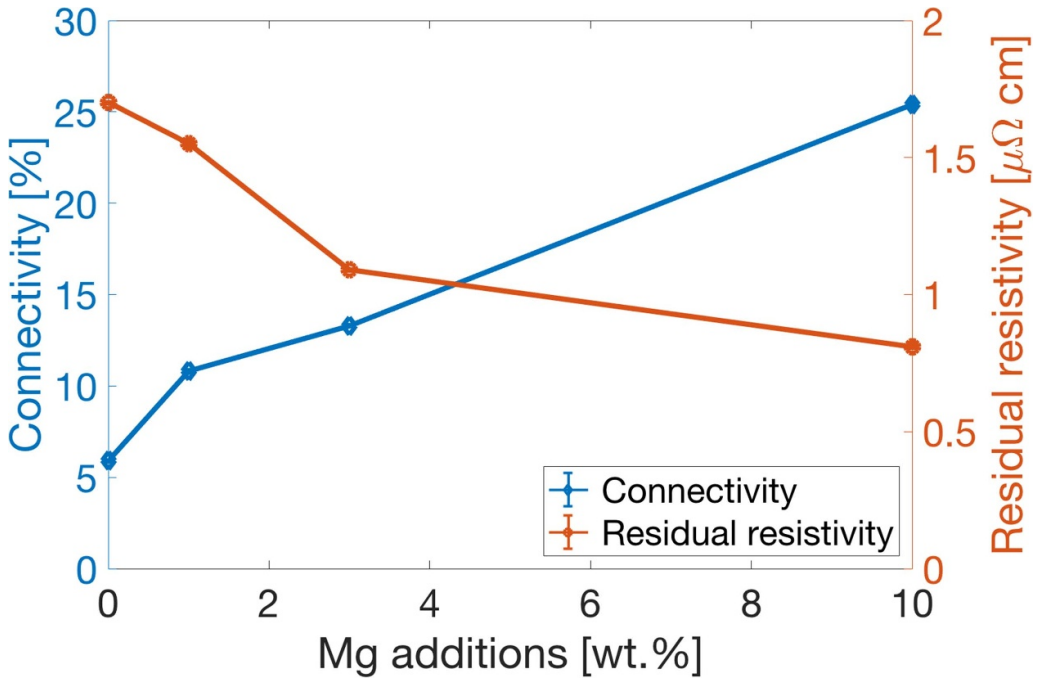

Figure 9. Connectivity and residual resistivity of the bulk samples estimated from normal state electrical transport measurements following the analysis outlined by Collings *et al* [28].

4. Conclusion

This work introduced a novel LPS process that we developed to improve the connectivity of *ex-situ* MgB_2 bulks. Mg additions (1–10 wt.%) were mixed to pre-synthesised MgB_2 to make composite powders that were sintered at 900 °C by FAST. Mg had a very substantial effect on the density of the bulks and their composition. Density increased from 68% to 79% and the fraction of MgB_4 was reduced from 11 to ∼0 wt.% by adding 10 wt.% Mg to unmodified MgB_2. Pressure and dilatometry data recorded *in-situ* during the sintering process revealed that Mg additions led to different mechanisms depending on the Mg fraction. For small Mg fractions (1 wt.%) all the metallic Mg evaporated during sintering and generated a positive $Mg_{(g)}$ pressure which modified the dynamic equilibrium of the MgB_2 decomposition reaction causing less MgB_4 to be formed. No liquid phase was formed and thus no increase in density was observed. For intermediate Mg fractions (3 wt.%) some Mg evaporated and MgB_2 decomposition was suppressed. A liquid phase was formed, enhancing densification and reacting with pre-existing MgB_4 to form 'fresh' MgB_2. No residual Mg was detected and the density increased compared to unmodified MgB_2. For large Mg fractions (6 and 10 wt.%) more liquid phase was formed and led to further density improvements, and all pre-existing MgB_4 was transformed into MgB_2. A small amount of residual Mg remained in the bulks after the sintering process. Connectivity was also improved with Mg additions, increasing four fold in the 10 wt.% Mg-MgB_2 sample compared to unmodified MgB_2. J_c values at low field were also significantly improved by Mg additions, in particular the 6 and 10 wt.% Mg-MgB_2 specimens showed J_c(20 K, 0 T) values 4–5 times higher than for unmodified MgB_2. Matthews *et al* [11] obtained similar J_c values by sintering unmodified MgB_2 at 1200 °C (instead of only 900 °C in this study), suggesting that Mg additions enabled the production of well connected bulks at much lower temperatures. The optimal amount of Mg additions is the stoichiometric quantity needed to fully react with all the pre-existing MgB_4 in the MgB_2 powder, which was found to be around 6 wt.% for the MgB_2 powder used in this study.

The LPS method developed in this work provides a practical alternative to the conventional *ex-situ* process by allowing well connected and MgB_4-free bulks to be manufactured at lower temperatures, minimising the detrimental effect of coarsening, improving the production rate and significantly reducing the production costs.

Acknowledgments

The Authors would like to thank the UK Engineering and Physical Science Research Council and the Department of Materials, University of Oxford for financial support (EP/P026427/1, EP/ M508111/1, Manufacture using Advanced Powder Processes and Process). The Authors acknowledge the use of characterisation facilities within the David Cockayne Centre for Electron Microscopy, Department of Materials, University of Oxford. The data are available at https://doi.org/10.5287/bodleian:xr11rwggY.

ORCID iDs

G A B Matthews https://orcid.org/0000-0002-6352-8596
C R M Grovenor https://orcid.org/0000-0001-6425-354X
S Speller https://orcid.org/0000-0002-6497-5996

References

[1] Buzea C and Yamashita T 2001 Review of superconducting properties of MgB_2 *Supercond. Sci. Technol.* **14** 1–35

[2] Durrell J H, Ainslie M D, Zhou D, Vanderbemden P, Bradshaw T, Speller S, Filipenko M and Cardwell D A 2018 Bulk superconductors: a roadmap to applications *Supercond. Sci. Technol.* **31** 103501

[3] Moseley D, Matthews G A B M, Zhou D, Cientanni V, Tsui Y, Ainslie M D, Speller S C and Durrell J H 2021 Improved pulsed field magnetisation in MgB_2 trapped-field magnet *Supercond. Sci. Technol.* **34** 085018

[4] Pan A V, Zhou S, Liu H and Dou S 2003 Properties of superconducting MgB_2 wires: *in situ* versus *ex situ* reaction technique *Supercond. Sci. Technol.* **16** 639–44

[5] Dancer C E J, Prabhakaran D, Başoğlu M, Yanmaz E, Yan H, Reece M, Todd R I and Grovenor C R M 2009 Fabrication and properties of dense *ex situ* magnesium diboride bulk material synthesized using spark plasma sintering *Supercond. Sci. Technol.* **22** 095003

[6] Yamamoto A, Tanaka H, Shimoyama J I and Ogino H 2012 Towards the realization of higher connectivity in MgB_2 conductors: *in-situ* or sintered *ex-situ? Jpn. J. Appl. Phys.* **51** 010105

[7] Schmidt Jurgen, Schnelle W, Grin Y and Kniep Rudiger 2003 Pulse plasma synthesis and chemical bonding in magnesium diboride *Solid State Sci.* **5** 535–9

[8] Lee S Y, Yoo S I, Kim Y W, Hwang N M and Kim D Y 2003 Preparation of dense MgB_2 bulk superconductors by spark plasma sintering *J. Am. Ceram. Soc.* **86** 1800–2

[9] Häßler W, Scheiter J, Hädrich P, Kauffmann-Weiß S, Holzapfel B, Oomen M and Nielsch K 2018 Properties of *ex-situ* MgB_2 bulk samples prepared by uniaxial hot pressing and spark plasma sintering *Physica* C **551** 48–54

[10] Aldica G, Popa S, Enculescu M, Pasuk I, Ionescu A M and Badica P 2018 Dwell time influence on spark plasma-sintered MgB_2 *J. Supercond. Novel Magn.* **31** 317–25

[11] Matthews G A B, Grovenor C R M, Speller S and Grant P S 2020 Effect of the sintering temperature on the microstructure and superconducting properties of MgB_2 bulks manufactured by the field assisted sintering technique *Supercond. Sci. Technol.* **33** 054003

[12] Batalu D, Aldica G, Popa S, Kuncser A, Mihalache V and Badica P 2015 GeO_2 -added MgB_2 superconductor obtained by spark plasma sintering *Solid State Sci.* **48** 23–30

[13] Liu Z-kui, Schlom D G, Li Q and Xi X X 2001 Thermodynamics of the Mg–B system: implications for the deposition of films thermodynamics of the Mg–B system: implications for the deposition of MgB_2 thin films *Appl. Phys. Lett.* **78** 3678

[14] Kario A, Nast R, Häler W, Rodig C, Mickel C, Goldacker W, Holzapfel B and Schultz L 2011 Critical current density enhancement in strongly reactive *ex situ* MgB_2 bulk and tapes prepared by high energy milling *Supercond. Sci. Technol.* **24** 075011

[15] Takano Y, Takeya H, Fujii H, Kumakura H, Hatano T, Togano K, Kito H and Ihara H 2001 Superconducting properties of MgB_2 bulk materials prepared by high-pressure sintering *Appl. Phys. Lett.* **78** 2914–16

[16] Jung C U, Park M S, Kang W N, Kim M S, Kim K H P, Lee S Y and Lee S I 2001 Effect of sintering temperature under high pressure on the superconductivity of MgB_2 *Appl. Phys. Lett.* **78** 4157–9

[17] Ma H A *et al* 2002 Superhard MgB_2 bulk material prepared by high-pressure sintering *J. Phys. Condens. Matter* **14** 11181–4

[18] Katzman H 1971 Sintered diamond compacts with a cobalt binder *Science* **172** 1132–4

[19] Zhao H and Cheng Y-bing 1999 Formation of TiB_2-TiC composites by reactive sintering *Ceram. Int.* **25** 353–8

[20] German R M 2009 Review: liquid phase sintering *J. Mater. Sci.* **44** 1–39

[21] Zeng R, Lu L, Wang J L, Horvat J, Li W X, Shi D Q, Dou S X, Tomsic M and Rindfleisch M 2007 Significant improvement in the critical current density of *in situ* MgB_2 by excess Mg addition *Supercond. Sci. Technol.* **20** 1–6

[22] Zeng R *et al* 2008 Excess Mg addition MgB_2/Fe wires with enhanced critical current density *J. Appl. Phys.* **103** 083911

[23] Ma Z, Liu Y, Cai Q and Liming Y 2014 Significant improvement in the critical current density of MgB_2 bulks *in situ* sintered at low temperature by excess Mg addition *Physica* C **496** 49–52

[24] Zhang H, Zhao Y and Zhang Y 2015 The effects of excess Mg addition on the superconductivity of MgB_2 *J. Supercond. Novel Magn.* **28** 2711–4

[25] Güner S B, Savaşkan B, Öztürk K, Çelik Ş, Aksoy C, Karaboğa F, Koparan E T and Yanmaz E 2019 Investigation on superconducting and magnetic levitation force behaviour of excess Mg doped-bulk MgB_2 superconductors *Cryogenics* **101** 131–6

[26] Hill J and Howard J 1987 Quantitative phase analysis from neutron powder diffraction data using the Rietveld method *J. Appl. Crystallogr.* **20** 467–74

[27] Bean C P 1962 Magnetization of hard superconductors *Phys. Rev. Lett.* **8** 250–3

[28] Collings E W, Sumption M D, Bhatia M, Susner M A and Bohnenstiehl S D 2008 Prospects for improving the intrinsic and extrinsic properties of magnesium diboride superconducting strands *Supercond. Sci. Technol.* **21** 103001

[29] Eltsev Y, Lee S, Nakao K, Chikumoto N, Tajima S, Koshizuka N and Murakami M 2002 Anisotropic superconducting properties of MgB_2 single crystals probed by in-plane electrical transport measurements *Phys. Rev.* B **65** 140501(R)

[30] Coleman F F and Egerton A 1935 A study of the vapour pressures of magnesium, thallium and zinc and the determination of their chemical constants *Phil. Trans. R. Soc.* A **234** 177–204

[31] Moser Z *et al* 1998 New thermodynamic data for liquid Aluminum-Magnesium alloys from emf, vapor pressures and calorimetric studies *J. Phase Equilib.* **19** 38–47

[32] Falk L K L 2004 Imaging and microanalysis of liquid phase sintered silicon-based ceramic microstructures *J. Mater. Sci.* **39** 6655–73

[33] Anderson P W 1959 Theory of dirty superconductors *J. Phys. Chem. Solids* **11** 26–30